Coupled (H^+, M^{3+}) substitutions in forsterite

Feiwu Zhang and Kate Wright

Nanochemistry Research Institute, Curtin University of Technology, PO Box U1987, Perth 6845, WA Australia

Abstract

Coupled substitutions involving hydrogen plus trivalent elements (Al, Eu, Fe, Ga, Gd, Lu, Mn, Nd, Pu, Sc, Y and Yb) in forsterite (Mg_2SiO_4) are studied using atomistic simulation methods. Incorporation of hydrogen is energetically favourable when included in the forsterite lattice as hydroxyl groups (OH^-) at O3 sites while the trivalent cations replace either magnesium or silicon. Our calculations show a strong dependence on the ionic radius of the impurity species and some variation with pressure. There are also significant structural distortions around the impurity defects. At low pressure (0 GPa), the smaller trivalent cations, (eg. Al, Fe, Mn and Ga) substitute into forsterite by replacing Si as: $M'_{Si} + OH^{\bullet}_{O3}$. The larger trivalent cations (eg. Eu, Gd, Lu, Nd, Pu, Y and Yb) however, replace Mg at the M2 site coupled with an Mg1 vacancy as described by $V''_{Mg1} + M^{\bullet}_{Mg2} + OH^{\bullet}_{O3}$. At 12 GPa, the large cations are more stable at Mg1 relative to Mg2, but both are predicted to be less stable than configurations associated with Si vacancies. The trivalent ionic radius has a significant effect on the H incorporation mechanism, however, the high formation energy of Si vacancies suggests that the presence of H in forsterite could inhibit incorporation of these elements, particularly at high pressure.

1. INTRODUCTION

Olivine [$(MgFe)_2SiO_4$] is a major component of the Earth's upper mantle and an important potential reservoir of H and thus water in the Earth's interior. The mechanisms of water incorporation, as H defects, have been extensively studied (e.g. Walker et al., 2007; Bali et al., 2008) because of their influence on the physical properties of forsterite, and on the rheological behavior of the Earth's upper mantle (Katayama and Karato, 2008). Information from samples of mantle-derived olivines (Dreibus et al., 1995; Kent and Rossman, 2002), experiments on synthetic forsterite (Grant et al., 2006), and computer simulations (Brodholt and Refson, 2000; Walker et al., 2006), all show that water can be incorporated into the crystal structure as H defects associated with either Mg and/or Si vacancies. The defect structure and hydration mechanisms of olivine have been studied by single-crystal X-ray diffraction, and by Infra-red (IR) spectroscopy. The X-ray structure refinements of hydrous olivine show evidence for Mg^{2+} vacancies (Smyth et al., 2006) whilst IR spectroscopy provides evidence for H associated with Mg^{2+} vacancies (Mosenfelder et al., 2006), as well as for hydration mechanisms involving both Mg^{2+} and Si^{4+} vacancies, depending on experimental conditions (Lemaire et al., 2004; Litasov et al., 2007). Simulations (See Wright, 2006 for review) show that on energetic grounds, H is most easily incorporated into pure forsterite in association with Si vacancies. However, H concentration levels in the Earth's mantle are still unknown.

Trace elements in the mantle (e.g. Ti (Walker et al., 2007)) may also influence the ability of nominally anhydrous minerals such as olivine to host H and thus influence its distribution in mantle silicates. Trace and rare earth element incorporation in olivine, orthopyroxene and clinopyroxene has been extensively studied, particularly

in relation to mineral/melt partitioning (e.g. Colson et al., 1988, 1989; Beattie, 1994; Evans et al., 2008). Two charge compensating mechanisms for M^{3+} incorporation have been proposed: in the first, M^{3+} is charge balanced by the formation of cation vacancies; and in the second, by coupled substitution. Experiments by Evans et al (2008) indicated that Al^{3+} incorporation occurred by substitution at both tetrahedral and octahedral sites, i.e. $(Al_{Mg} + Al_{Si})$. Purton et al (1997) calculated solution energies for impurity incorporation in forsterite and found that the most favourable mechanism involved M^{3+} substitution at Mg2 sites, charge balanced by Na^{+} at Mg1. Subsequent experiments (Grant and Wood, 2006) have confirmed that adding Na to their starting materials, led to increased uptake of trace elements by olivine. Thus it would appear that mixed valence coupled substitution mechanisms are favourable for trace element incorporation. What we wish to determine in this study is if this supposition holds true in the case where the monovalent species is hydrogen.

Experimental and theoretical studies dealing with possible H/trace element couples are much more limited. Berry et al (2007) identified the vibrational spectra of OH associated with a number of trivalent cations, however only a limited number of such impurities (Fe, Richmond and Brodholt, 2000; Cr, Dudnikova et al., 2003) have been examined by computational methods. In this study we use atomistic simulation methods to investigate relationships between a range of M^{3+} impurity ions (Al, Fe, Ga, Mn, Sc, Lu, Yb, Y, Gd, Eu, Nd and Pu) in combination with H in forsterite, the Mg end member olivine. The aim is to obtain quantitative estimates of the stability of trivalent element associated with hydrogen in forsterite at upper mantle pressures and the

corresponding substitution mechanisms. Here we report calculated atomic geometries, defect energetics and reaction enthalpies of 12 trivalent elements + H defect complexes in forsterite. The results, when combined with experimental information (Berry et al., 2007), can be used to enhance our knowledge of the behaviour of trace elements and their relationship to H defects in the Earth's upper mantle.

2. METHODOLOGY

In this work, defects in forsterite are studied by atomistic simulation techniques, based on the Born model of solids that employs interatomic potential functions to describe the energy of the system in terms of the atomic coordinates. All calculations were performed with the General Utility Lattice Program (GULP) code (Gale, 1997). We use a potential set based on parameters for oxides (Catlow, 1977; Sanders et al., 1984; Lewis and Catlow, 1985), that have previously been used to study H uptake mechanisms in forsterite, wadsleyite (Walker et al., 2006) and pyroxenes (Gatzemeier and Wright, 2006). Full details of these parameters can be found in Walker et al (2006). Interactions between the trivalent impurities and oxygen in the forsterite lattice are calculated using potential parameters detailed elsewhere in the literature (Lewis and Catlow, 1985; Lewis et al., 1995; Purton et al., 1997). Further parameters for the hydroxyl-oxygen M^{3+} impurity interactions were modified according to the methodology given in Schröder at al (1992). The full set of impurity-oxygen parameters are given in Table 1.

To treat the hydroxyl groups, we used the Morse potential:

$$U_{ij}^{More} = D\{[1-\exp(-a(r-r_0))]^2 - 1\} \quad (1)$$

where D (7.0525 eV) corresponds to the dissociation energy of the bond, r_0 (0.9485 Å) is the equilibrium bond length and a (2.03 $Å^{-1}$) is fitted to experimental data and related to the vibrational frequency of the stretching mode. These parameter values and the short range Morse cut-off (1.3 Å) are the same as in Walker et al. (2006).

The energy cost of introducing a point defect (vacancy, interstitial, or impurity) into a solid can be determined by either a cluster method, or by the use of a large supercell. In this study we use the latter method, with a perfect forsterite supercell (4 x 2 x 4) containing 128 formula units and having a cell volume of approximately 9384 $Å^3$, which is sufficient to minimise the effect of defect-defect interactions in periodic images. The use of the supercell approach also facilitates the determination of pressure effects on defect processes. The defect formation energy (E_{DF}) is then the energy difference between the pure and defective cells.

When a trivalent cation is introduced into the forsterite lattice, it will sit either at a Mg (M1 or M2) site or at a Si site. Calculated binding energies (Braithwaite et al., 2003) suggest that hydroxyl groups are strongly bound to vacancies and thus are likely to be coupled to any defect causing a local charge imbalance. Therefore the trivalent impurities are introduced into the forsterite lattice adjacent to H defects. Calculations have been carried out at simulated pressures of 0 and 12 GPa, and full relaxation (lattice parameters and atomic positions) of the perfect and defective structures is allowed in the calculation at both pressures.

3. RESULTS AND DISCUSSION

3.1. Pure forsterite

The crystal structure of forsterite (Fig. 1a) consists of independent SiO_4 tetrahedra linked by the divalent cations in six-fold oxygen coordination with space group Pbnm. There are two symmetry-distinct octahedral Mg sites in the forsterite structure: M1 at the inversion site and the larger M2 at the mirror site; one distinct tetrahedral Si site which lies on the mirror plane; and three distinct oxygen sites, (O1 and O2 on the mirror plane and two O3 in the general position).

The Birch-Murnaghan equation of state parameters were determined to be K_0 = 148.8 GPa and K_0' = 4.05 which compares reasonably well with experimental values of 125.0 GPa and 4.0 (Downs et al., 1996) and 135 GPa and 4.9 from Density Functional Theory calculations (Wentzcovitch and Stixrude, 1997). Over the pressure range 0 – 12 GPa, the calculated volume changes by 6.8%, contracting from 293.2 $Å^3$/cell to 273.4 $Å^3$/cell, which is a good agreement with previous experimental measurements (Downs et al., 1996). Locally, the compressibility of the different cation sites varies, with Mg2 being the most compressible site under pressure, and Si the least, in agreement with previous ab initio simulations (Wentzcovitch and Stixrude, 1997).

3.2. Incorporating impurities

M^{3+} impurities, and associated H, can be incorporated into the forsterite lattice via a number of mechanisms. Firstly, we can have substitution of an M^{3+} impurity at either an Mg1 or Mg2 site, accompanied by a Mg vacancy and a hydroxyl group at an oxygen site.

In defect notation this is written as $[V''_{Mg} + M^{\bullet}_{Mg} + OH^{\bullet}_{O3}]$. Secondly, trivalent cations may substitute onto the Si site, with an accompanying hydroxyl: $[M'_{Si} + OH^{\bullet}_{O3}]$. The structure of both defect clusters is illustrated in Fig. 1b and 1c respectively.

Calculations were performed at 0 GPa and 12 GPa to determine the structure and energy of the different defect complexes and to assess the influence of pressure on incorporation mechanisms. To illustrate the different energies associated with different defect configurations at 0 GPa, we present the defect formation energies (E_{DF}) for all possible Al^{3+}- H^{+} defect complexes in Table 2. Results for all other M^{3+}cations studies are available in the supplementary data. From Table 2 we see that the M^{3+} cation has a lower substitution energy when placed on the Mg2 rather than Mg1 site, in agreement with the calculations of Purton et al (1997). Furthermore, this configuration is predicted to be most favourable when accompanied by an adjacent Mg1 vacancy with a hydroxyl at O3 (i.e. Fig. 1b).

The values of E_{DF} for all cations considered is shown in Fig. 2a-c for the substitutions MVM1 ($V''_{Mg1} + M^{\bullet}_{Mg1} + OH^{\bullet}_{O3}$, Mg vacancy mechanism 1) MVM2 ($V''_{Mg1} + M^{\bullet}_{Mg2} + OH^{\bullet}_{O3}$, Mg vacancy mechanism 2) and SVM ($M'_{Si} + OH^{\bullet}_{O3}$, Si vacancy mechanism). The energies at 0 GPa increase steadily with increasing ionic radius for all three mechanisms. In all cases, the MVM2 defect has the lowest defect energy of the three mechanisms. It is important to stress that E_{DF} is the difference between the energy of the defective and pure cell and does not take into account any solution reactions. Thus the magnitude of E_{DF} reflects the degree of lattice relaxation required to accommodate the defect.

The effects of pressure on impurity incorporation are variable, depending on the particular species. At 12 GPa the same general trend of increasing enthalpy with ionic radius at all substitution sites is observed (Fig. 2a-c). However, the Mg1 site substitution is energetically more favourable than Mg2 for larger cations: Gd, Eu, Nd, Pu. Fig. 2d shows the enthalpy difference between the MVM1 and MVM2 at 12 GPa. This change in Mg site preference is only seen when hydrogen is present, as for anhydrous substitutions, the Mg2 site continues to be the most favourable (Table 3). Thus, in Mg deficient forsterite, as shown in Fig. 2d, the larger cations will partition into the Mg1 site at high pressure while the smaller cations remain associated with Mg2. It is possible that this behaviour is due to changes in local structure around the defect, and to variability in compressibility of the two sites. The Mg2 site, although larger at 0 GPa than Mg1, is more compressible. The influence of these defects on structure is described later in this section.

3.3. Stability of impurity defects

The relative stability of the different defect sites can be determined by calculating solution reactions between forsterite, water and the different component oxide phases as in the work of Purton et al. (1997), or by considering the relative defect incorporation energies. The first method requires a choice of oxide, and energy terms to describe the dissociation of water and formation of OH groups in the structure. A value for this proton transfer reaction was calculated at 0 GPa by Wright and Catlow (1994), but no value is available for the same reaction at higher pressure. Thus, we use the second simpler

method, which requires only the defect formation energies, to calculate the reaction enthalpies (ΔH) of the following equations at 0 and 12 GPa:

$$Mg_2(Si_{1-x}M_x)O_{4-x}(OH)_x + xMg_2SiO_4 \rightarrow (Mg_{1-2x}M_x)MgSiO_{4-x}(OH)_x + 4xMgO \quad (2)$$

$$Mg_2(Si_{1-x}M_x)O_{4-x}(OH)_x + 4xMgSiO_3 \rightarrow (Mg_{1-2x}M_x)MgSiO_{4-x}(OH)_x + 3xMg_2SiO_4 \quad (3)$$

where, for this size of supercell, x equates to a value of 0.78 mol % and M^{3+} can be at the Mg1 site (MVM1) or the Mg2 site (MVM2). Each side of Equation 2 and 3 contains the same amount of each species and therefore we can compare the different defect configurations. Positive values of ΔH indicate a preference for the Si vacancy mechanism (SVM) while negative values favour Mg vacancies (MVM).

The calculated reaction energies at 0GPa are plotted in Fig. 3a and 3b. The results show that the smaller cations (Al, Fe Mn and Ga) with radii less than that of Sc, substitute for Si, associated with H for charge balance; while the larger trivalent cations (Lu, Yb, Y, Gd, Eu, Nd and Pu) replace Mg at the M2 site associated with additional H_{Mg1}. This is not surprising given the larger volume of the Mg2 site. Sc, which has an ionic radius close to that of Mg, can substitute into either the Mg2 or Si site without an obvious energy penalty. The effect of $MgSiO_3$ vs. MgO buffering is to shift the energies downwards by approximately 0.8 eV.

At 12 GPa, all values of ΔH are positive as shown in Figures 3c and 3d. For the SVM vs. MVM1 plot, the values show a strong tendency for Al and Ga to partition to the Si site, which decreases steadily for the larger cations. In the SVM vs. MVM2 case the profile is

quite different; Al and Ga still partition to Si but Sc now has the lowest value of ΔH and the larger cations appear to show preference for Si as well. Reaction enthalpies are shifted ~ 0.2 eV depending on the buffer, but this time they are higher for the $MgSiO_3$ buffered case.

We have also considered two substitution mechanisms for Al that are intermediate to the mechanisms discussed above, but have the ability to incorporate larger numbers of protons. These can be described as $[Al'_{Si} + V''_{Mg} + 3OH^{\bullet}_{O3}]$ and $[Al^{\bullet}_{Mg} + V''''_{Si} + 3OH^{\bullet}_{O3}]$. However, the resulting reaction energies are high and thus likely to be unstable relative to the simpler defects with either isolated Mg vacancy or Si vacancy proton incorporation mechanisms.

3.4. Anhydrous incorporation

Experimental evidence (Evans et al. 2008) suggests that trivalent cations such as Al^{3+} will substitute into anhydrous (dry) forsterite by coupled substitution as $[M'_{Si} + M^{\bullet}_{Mg}]$. We have calculated the Mg1 vs. Mg2 site preference for all M^{3+} cations in anhydrous forsterite at both 0 and 12 GPa. The results imply that at both pressures, all M^{3+} ions considered are more energetically favoured at the Mg2 rather than Mg1 site when coupled with the Si site substitution. This is in contrast to the hydrous system where, as discussed in 3.2 section, the Mg1 site substitution becomes more favourable than Mg2 for larger cations (Gd, Eu, Nd and Pu) at 12 GPa.

From the above, it would appear that the presence of H influences the site preference of large M^{3+} cations at high pressure, but, do these impurities facilitate H incorporation?

One way to assess this is to compare M^{3+} containing forsterite plus hydrous forsterite with that containing the coupled ($M^{3+}H^{+}$). This is expressed below in Equations 4 (forsterite + MgO) and 5 (forsterite + $MgSiO_3$). For Al, we can write:

$$[Al_{Mg}^{\bullet} - Al_{Si}^{'}] + [V_{Mg}^{''} - 2OH^{\bullet}] + 4 \cdot MgO \rightarrow 2 \cdot [Al_{Si}^{'} - OH^{\bullet}] + Fo \quad (4a)$$

Where a corresponding energy is calculated from:

$$E = 2 \cdot E(Al_{Si}^{'} - OH^{\bullet}) + U_{Mg_2SiO_4} - E(Al_{Mg}^{\bullet} - Al_{Si}^{'}) - E(V_{Mg}^{''} - 2OH^{\bullet}) - 4 \cdot U_{MgO} = -1.22 \ eV \quad (4b)$$

For the enstatite buffered system we have:

$$[Al_{Mg}^{\bullet} - Al_{Si}^{'}] + [V_{Mg}^{''} - 2OH^{\bullet}] + 3 \cdot Fo \rightarrow 2[Al_{Si}^{'} - OH^{\bullet}] + 4 \cdot Ens \quad (5a)$$

with the energy calculated from

$$E = 2 \cdot E(Al_{Si}^{'} - OH^{\bullet}) + 4 \cdot U_{MgSiO_3} - E(Al_{Mg}^{\bullet} - Al_{Si}^{'}) - E(V_{Mg}^{''} - 2OH^{\bullet}) - 3 \cdot U_{Mg_2SiO_4} = -0.37 \ eV \quad (5b)$$

The reaction energies show a clear binding energy between trivalent substitution and OH groups and indicate that Al will facilitate incorporation of H when substituting at the Si site. If we assume that OH is present in the hydrogarnet type defect, the second term on the left hand side of Equations 4a and 5a is $[V_{Si}^{''''} - 4OH^{\bullet}]$. If this reacts with Al to give $2 \cdot [V_{Mg}^{''} - 2OH^{\bullet}]$ then there is an additional energy penalty that is large and positive (4.29 eV and 3.45 eV for MgO and Enstatite buffered case respectively). Substitution of larger cations for Al in Equations 4a and 5a decreases the binding energy between M^{3+} and H as a function of ionic radius. Values for the energy terms for reaction 4b (and 5b) are Sc = -1.13 (-0.28), Y= -0.70 (+0.18) and Pu = -0.72 (+0.13).

Previous calculations (Brodholt and Refson, 2000; Braithwaite et al., 2003; Walker et al., 2006) all predicted that formation of the hydrogarnet defect would be the most effective means of incorporating water into the forsterite lattice. The results above support this scenario, but also show that incorporation in association with trivalent impurities will be more effective than a mechanism associated with Mg vacancies. This model is consistent with results from recent experimental work (Kovács et al., 2010).

3.5. Influence on structure

Incorporation of defects into the forsterite lattice leads to local distortion of the structure, where the degree of distortion varies with ion size. For example, the Al substitution $[Al'_{Si} + OH^{\bullet}_{O3}]$ causes the three O-Al distances to increase by 6% relative to Si in pure forsterite, and the Al-O_{OH} distance to increase by twice that amount. For M^{3+} substitutions above an ionic radius of 0.8 Å, the terahedra begin to show signs of "flattening", as illustrated in Fig. 4, where the YbOH and PuOH structures are presented and the AlOH structure is also included for comparison. At 12 GPa, the structures are essentially unchanged although M – $O_{(OH)}$ distances decrease slightly for Al (1.84Å) and Yb (2.03Å) while Pu– $O_{(OH)}$ remains constant. The similarity in structures and bond lengths reflects the relative incompressibility of this tetrahedral unit with pressure.

To determine structural differences in the $[V''_{Mg} + M^{\bullet}_{Mg} + OH^{\bullet}_{O3}]$ defect, we have compared the mean M^{3+}- Si and M^{3+}-Mg distances from the first coordination shell. When M^{3+} replaces Mg2, the Si – M^{3+} and Mg1 – M^{3+} distances increase smoothly with increasing ionic radii while the Mg2 – M^{3+} distances essentially remain constant at 3.93 Å (0 GPa)

and 3.85 Å (12 GPa). The trend is similar for M^{3+} - Mg2 and M^{3+} - Si, when M^{3+} is at an Mg1 site with an adjacent Mg1 vacancy, although there is a sharp increase in M^{3+} - Mg1 mean distance of ~0.6 Å at M^{3+} ionic radii above 0.85Å. O-H distances remain almost constant (0.97 – 1.00 Å) in both defects types across the whole series of impurities.

3.6. Comparison with experiment

Experimental data for coupled impurity incorporation in forsterite or olivine is limited. The experimental observations described in Taura et al (1998), report partition coefficients between dry olivine and melt for 27 trace elements at upper mantle conditions of 3 to 14 GPa. The authors find that the Al^{3+} abundance in the Si site is not dependent on pressure, but the Al^{3+} abundance in the Mg site increases with pressure while the partition coefficients of other larger trivalent cations, which occupy the Mg site, decrease with pressure. Our simulations show for both Mg vacancy substitution mechanisms (MVM1 and MVM2), E_{DF} decreases with pressure for the small trivalent cations Al and Ga, stays the same for Fe and Mn, but increases for all cations with ionic radius greater than that of Mg (Fig. 2a and 2b). No such dependence was found for the Si vacancy substitution mechanism, in agreement with the experimental results.

Evans et al. (2008) investigated partitioning of Y, Sc, Zr and Al between melt and anhydrous forsteritic olivine. Their results indicated a coupled substitution mechanism for Al i.e. $Al'_{Si} + Al^{\bullet}_{Mg}$, a vacancy mechanism (e.g. $2M^{\bullet}_{Mg} + V''_{Mg}$) for Y, and somewhat anomalous behaviour for Sc. The behaviour of Al is in agreement with earlier work of Colson et al. (1989) who also investigated incorporation of Sc, Yb and Cr in olivine, predicting that all three of these larger species would be charge balanced by Mg

vacancies. At 0GPa, where M^{3+} is charge balanced by H, our simulations show the same site preference for the smaller cations (Si site) and larger cations (Mg site) as the anhydrous experiments above. Sc appears to be able to substitute into either site with ease which could explain the inconsistent behaviour observed by Evans et al. (2008). Beattie (1994) investigated trace element partitioning between olivine and melt and concluded that REEs would most likely substitute for Mg, charge balanced by Al at Si sites. However, such mechanisms will be dependent on the activity of Al and Si in the system. The computational results of Purton et al. (1997) on anhydrous forsterite do not support the above analyses, but predict that M^{3+} will always substitute for Mg2 and that solution energies will be dependent on the nature of the charge compensating species. The most favourable defect configuration suggested a coupled M^{3+} substitution with Na^{+} as charge compensation.

Investigations of trivalent element incorporation in forsterite in the presence of water are even more limited. Berry et al (2007) measured the infrared (IR) signature of a range of elements, including Al, Mn, Ga, Y, and Lu, in hydrous forsterite synthesized at 1.5 GPa and 1400 ˚C but did not speculate widely on the associated defect configurations. Their results are interpreted in terms of a defect model where the most important mechanism involves M^{3+} at Mg2, associated with an adjacent Mg1 vacancy and OH group, i.e. the same as our MVM2 model. However, Berry et al (2007) did not find the evidence for the coupled substitution of H^{+} and small M^{3+} for Si^{4+} and these authors also note the need for atomistic calculations to clarify defect configurations unambiguously.

4. CONCLUSIONS

Understanding the evolution and composition of the Earth requires a detailed knowledge of the properties of geological materials under the conditions of the Earth's deep interior. Olivine is volumetrically the most important silicate phase in the Earth's upper mantle and understanding the mechanisms by which trace elements and hydrogen partition into olivine is essential before a complete description of this part of the Earth can be made. In this study, coupled substitutions involving trivalent elements and hydrogen have been investigated using atomistic simulation methods at 0 and 12 GPa. Our results suggest that the most favourable incorporation mechanism for M^{3+}- H couples at low pressures is dependent on ionic radius, with smaller M cations partitioning into Si sites and those with radii larger than ~0.8 Å favouring the larger M2 site.

The application of pressure leads to a distortion and compression of the Mg2 site, such that, when Mg1 is vacant as in the MVM2 defect, the site is no longer able to accommodate the larger M cations. Thus MVM1 becomes more stable. Both are less stable at high pressure however, than SVM. The high formation energies of defects at the Si site may indicate that the presence of H will inhibit uptake of M^{3+}, particularly for those elements with large ionic radii. However, smaller cations such as Al, that partition strongly to Si sites, could enhance H incorporation in the Earth's upper mantle. Alternatively, defect incorporation may be favoured close to dislocation cores, or to grain boundaries, where the local structure is more distorted. The incorporated water may therefore affect the plastic deformation of Earth material. Of course factors such as the activity of water, concentration of impurities and other phases present in the system, will all play a role in determining defect behaviour in forsterite. There is a relationship

between the presence of H and the mechanisms by which olivine deforms in the mantle and this has implications for seismic anisotropy measured at the Earth's surface and the development and refinement of geodynamic models. Given the close relationship between H incorporation and trivalent elements substitutions in olivine under different conditions, our study has the potential to refine the understanding of mantle processes in different tectonic environments.

Acknowledgements. We thank the three anonymous reviewers and the associate editor, Dr. Michael Toplis, for their constructive comments. Thanks also to Steven Reddy and Julian Gale for fruitful discussions. This study was funded by ARC discovery project DP0878453. We thank iVEC and the NCI Facility, Australia for the provision of computing resources.

REFERENCES

Bali, E., Bolfan-Casanova, N., and Koga, K. T., 2008. Pressure and temperature dependence of H solubility in forsterite: An implication to water activity in the Earth interior. *Earth and Planetary Science Letters* **268**, 354-363.

Beattie, P., 1994. Systematics and energetics of trace-element partitioning between olivine and silicate melts: Implications for the nature of mineral/melt partitioning. *Chem. Geol.* **117**, 57-71.

Berry, A. J., O'Neill, H. S. C., Hermann, J., and Scott, D. R., 2007. The infrared signature of water associated with trivalent cations in olivine. *Earth and Planetary Science Letters* **261**, 134-142.

Braithwaite, J. S., Wright, K., and Catlow, C. R. A., 2003. A theoretical study of the energetics and IR frequencies of hydroxyl defects in forsterite. *Journal of Geophysical Research-Solid Earth* **108**, 9.

Brodholt, J. P. and Refson, K., 2000. An ab initio study of hydrogen in forsterite and a possible mechanism for hydrolytic weakening. *J. Geophys. Res.* **105**, 18977-18982.

Catlow, C. R. A., 1977. Oxygen incorporation in the alkaline earth fluorides. *J. Phys. Chem. Solids* **38**, 1131-1136.

Colson, R. O., McKay, G. A., and Taylor, L. A., 1988. Temperature and composition dependencies of trace element partitioning: olivine/melt and low-Ca pyroxene/melt. *Geochim. Cosmochim. Acta* **52**, 539-553.

Colson, R. O., McKay, G. A., and Taylor, L. A., 1989. Charge balancing of trivalent trace elements in olivine and low-Ca pyroxene - A test using experimental partitioning data. *Geochim. Cosmochim. Acta* **53**, 643-648.

Downs, R., Zha, C., Duffy, T., and Finger, L., 1996. The equation of state of forsterite to 17.2 GPa and effects of pressure media. *American Mineralogist* **81**, 51-55.

Dreibus, G., Jagoutz, E., and Wanke, H., 1995. Water in the Earth's mantle*6th International Kimberlite Conference*, Novosibirsk, Russia.

Dudnikova, V. B., Gaister, A. V., Zharikov, E. V., Gul'ko, N. I., Senin, V. G., and Urusov, V. S., 2003. Effect of compensation doping on chromium solubility in forsterite. *Inorg. Mater.* **39**, 845-850.

Evans, T. M., O'Neill, H. S. C., and Tuff, J., 2008. The influence of melt composition on the partitioning of REEs, Y, Sc, Zr and Al between forsterite and melt in the system CMAS. *Geochim. Cosmochim. Acta* **72**, 5708-5721.

Gale, J. D., 1997. GULP: A computer program for the symmetry-adapted simulation of solids. *Journal of the Chemical Society-Faraday Transactions* **93**, 629-637.

Gatzemeier, A. and Wright, K., 2006. Computer modelling of hydrogen defects in the clinopyroxenes diopside and jadeite. *Physics and Chemistry of Minerals* **33**, 115-125.

Grant, K. J., Kohn, S. C., and Brooker, R. A., 2006. Solubility and partitioning of water in synthetic forsterite and enstatite in the system MgO-SiO_2-H_2O +/- Al_2O_3. *Contributions to Mineralogy and Petrology* **151**, 651-664.

Grant, K. J. and Wood, B. J., 2006. Trace element substitution mechanisms in olivine. *Geochim. Cosmochim. Acta* **70**, A212-A212.

Katayama, I. and Karato, S. I., 2008. Effects of water and iron content on the rheological contrast between garnet and olivine. *Physics of the Earth and Planetary Interiors* **166**, 57-66.

Kent, A. J. R. and Rossman, G. R., 2002. Hydrogen, lithium, and boron in mantle-derived olivine: The role of coupled substitutions. *American Mineralogist* **87**, 1432-1436.

Kovács, I., O'Neill, H. S. C., Hermann, J., and Hauri, E. H., 2010. Site-specific infrared O-H absorption coefficients for water substitution into olivine. *American Mineralogist* **95**, 292-299.

Lemaire, C., Kohn, S. C., and Brooker, R. A., 2004. The effect of silica activity on the incorporation mechanisms of water in synthetic forsterite: a polarised infrared spectroscopic study. *Contributions to Mineralogy and Petrology* **147**, 48-57.

Lewis, D. W., Catlow, C. R. A., Sankar, G., and Carr, S. W., 1995. Structure of iron-substituted ZSM-5. *J. Phys. Chem.* **99**, 2377-2383.

Lewis, G. V. and Catlow, C. R. A., 1985. Potential models for ionic oxides. *Journal of Physics C-Solid State Physics* **18**, 1149-1161.

Litasov, K. D., Ohtani, E., Kagi, H., Jacobsen, S. D., and Ghosh, S., 2007. Temperature dependence and mechanism of hydrogen incorporation in olivine at 12.5-14.0 GPa. *Geophysical Research Letters* **34**, 5.

Mosenfelder, J. L., Deligne, N. I., Asimow, P. D., and Rossman, G. R., 2006. Hydrogen incorporation in olivine from 2-12 GPa. *American Mineralogist* **91**, 285-294.

Purton, J. A., Allan, N. L., and Blundy, J. D., 1997. Calculated solution energies of heterovalent cations in forsterite and diopside: Implications for trace element partitioning. *Geochim. Cosmochim. Acta* **61**, 3927-3936.

Richmond, N. C. and Brodholt, J. P., 2000. Incorporation of Fe^{3+} into forsterite and wadsleyite. *American Mineralogist* **85**, 1155-1158.

Sanders, M. J., Leslie, M., and Catlow, C. R. A., 1984. Interatomic potentials for SiO_2. *J. Chem. Soc.-Chem. Commun.*, 1271-1273.

Schröder, K. P., Sauer, J., Leslie, M., Catlow, C. R. A., and Thomas, J. M., 1992. Bridging hydroxyl-groups in zeolitic catalysts – a computer-simulation of their

structure, vibrational properties and acidity in protonated faujasites (H-Y zeolites). *Chem. Phys. Lett.* **188**, 320-325.

Smyth, J. R., Frost, D. J., Nestola, F., Holl, C. M., and Bromiley, G., 2006. Olivine hydration in the deep upper mantle: Effects of temperature and silica activity. *Geophysical Research Letters* **33**.

Taura, H., Yurimoto, H., Kurita, K., and Sueno, S., 1998. Pressure dependence on partition coefficients for trace elements between olivine and the coexisting melts. *Physics and Chemistry of Minerals* **25**, 469-484.

Walker, A. M., Demouchy, S., and Wright, K., 2006. Computer modelling of the energies and vibrational properties of hydroxyl groups in alpha- and beta-Mg_2SO_4. *European Journal of Mineralogy* **18**, 529-543.

Walker, A. M., Hermann, J., Berry, A. J., and O'Neill, H. S., 2007. Three water sites in upper mantle olivine and the role of titanium in the water weakening mechanism. *Journal of Geophysical Research-Solid Earth* **112**.

Wentzcovitch, R. M. and Stixrude, L., 1997. Crystal chemistry of forsterite: A first-principles study. *American Mineralogist* **82**, 663-671.

Wright, K., 2006. Atomistic models of OH defects in nominally anhydrous minerals. *Reviews in Mineralogy and Geochemistry* **62**, 67-83.

Wright, K. and Catlow, C. R. A., 1994. A computer simulation study of (OH) defects in olivine. *Physics and Chemistry of Minerals* **20**, 515-518.

Tables

Table 1 Trivalent element related parameters of the potential model used in this study. The pair potentials are truncated beyond 12 Å.

	Buckingham potential		
Specials	A_1 (eV) M^{3+}-O^{2-}	A_2 (eV) M^{3+}-$O^{1.4-}$	ρ (Å)
Al	1460.30	1142.68	0.29912
Eu	1358.00	950.60	0.35560
Ga	1950.79	1365.56	0.28700
Gd	1336.80	935.76	0.35510
Fe	1102.40	876.60	0.32990
Lu	1347.10	942.97	0.34300
Mn	1257.90	880.53	0.32140
Nd	1379.90	965.93	0.36010
Pu	1376.20	963.34	0.35930
Sc	1299.40	909.58	0.33120
Y	1345.10	941.57	0.34910
Yb	1309.60	916.72	0.34620

Table 2. Total supercell and defect formation energies (E_{DF}) (eV) of Al^{3+} impurities in forsterite at 0 GPa

Configuration	Total energy of defective supercell	E_{DF}
Pure forsterite	-27198.88	-
$V''_{Mg1} + Al^{\bullet}_{Mg2} + OH^{\bullet}_{O1}$	-27194.74	4.14
$V''_{Mg1} + Al^{\bullet}_{Mg2} + OH^{\bullet}_{O2}$	-27193.19	5.69
$V''_{Mg1} + Al^{\bullet}_{Mg2} + OH^{\bullet}_{O3}$	-27195.42	3.46
$V''_{Mg1} + Al^{\bullet}_{Mg1} + OH^{\bullet}_{O3}$	-27194.80	4.08
$V''_{Mg2} + Al^{\bullet}_{Mg1} + OH^{\bullet}_{O1}$	-27192.66	6.22
$V''_{Mg2} + Al^{\bullet}_{Mg1} + OH^{\bullet}_{O2}$	-27192.34	6.54
$V''_{Mg2} + Al^{\bullet}_{Mg1} + OH^{\bullet}_{O3}$	-27193.40	5.48
$V''_{Mg2} + Al^{\bullet}_{Mg2} + OH^{\bullet}_{O3}$	-27194.57	4.31
$Al'_{Si} + OH^{\bullet}_{O1}$	-27148.36	50.52
$Al'_{Si} + OH^{\bullet}_{O2}$	-27149.20	49.68
$Al'_{Si} + OH^{\bullet}_{O3}$	-27149.60	49.28

Table 3 The Mg1 vs. Mg2 site preference in the coupled substitution of $[M'_{Si} - M^{\bullet}_{Mg}]$ in anhydrous forsterite at 0 and 12 GPa.

Specials	E_{DF} (eV) 0 GPa		H_{DF} (eV) 12 GPa	
	$[M'_{Si} - M^{\bullet}_{Mg\,1}]$	$[M'_{Si} - M^{\bullet}_{Mg\,2}]$	$[M'_{Si} - M^{\bullet}_{Mg\,1}]$	$[M'_{Si} - M^{\bullet}_{Mg\,2}]$
Al	13.44	13.10	13.63	12.97
Ga	14.56	14.15	14.78	13.83
Mn	22.55	21.83	22.83	22.31
Fe	23.26	22.54	23.54	23.03
Sc	29.39	28.71	30.32	29.47
Lu	37.05	36.18	38.11	37.49
Yb	37.83	37.00	38.85	38.47
Y	40.22	39.38	41.46	40.76
Gd	43.34	42.34	44.78	43.95
Eu	44.10	43.06	45.60	44.72
Nd	47.05	45.83	48.74	47.72
Pu	46.53	45.34	48.19	47.19

Figure captions

Figure 1 Perfect (a) and trivalent element M^{3+} bearing hydrous forsterite structures: $V''_{Mg1} + M^{\bullet}_{Mg2} + OH^{\bullet}_{O3}$ (b) and $M'_{Si} + OH^{\bullet}_{O3}$ (c).

Figure 2 Defect formation energies for trivalent element + H substitutions at 0 and 12 GPa: (a) MVM1: $V''_{Mg1} + M^{\bullet}_{Mg1} + OH^{\bullet}_{O3H}$; (b) MVM2: $V''_{Mg1} + M^{\bullet}_{Mg2} + OH^{\bullet}_{O3}$; (c) SVM: $M'_{Si} + OH^{\bullet}_{O3}$; and (d) relative Mg site preference. Above the y=0 line (positive values) Mg2 site is preferred for M^{3+}, below, Mg1 site is preferred.

Figure 3 Reaction energy ΔE of Equation 2 for MgO buffered system (dark square and solid line) and of Equation 3 for Enstatite $MgSiO_3$ buffered system (open circle and dots line) at pressure of 0 GPa (Fig. 3a, b); Reaction enthalpy ΔH of Equation 2 and 3 at pressure of 12 GPa (Fig. 3c, d).

Figure 4 Variation in structure of the ($M^{3+}H^{+}O_4$) tetrahedral with increasing M^{3+} ionic radius. M^{3+}- $O_{(OH)}$ distance are also shown for 0 GPa.

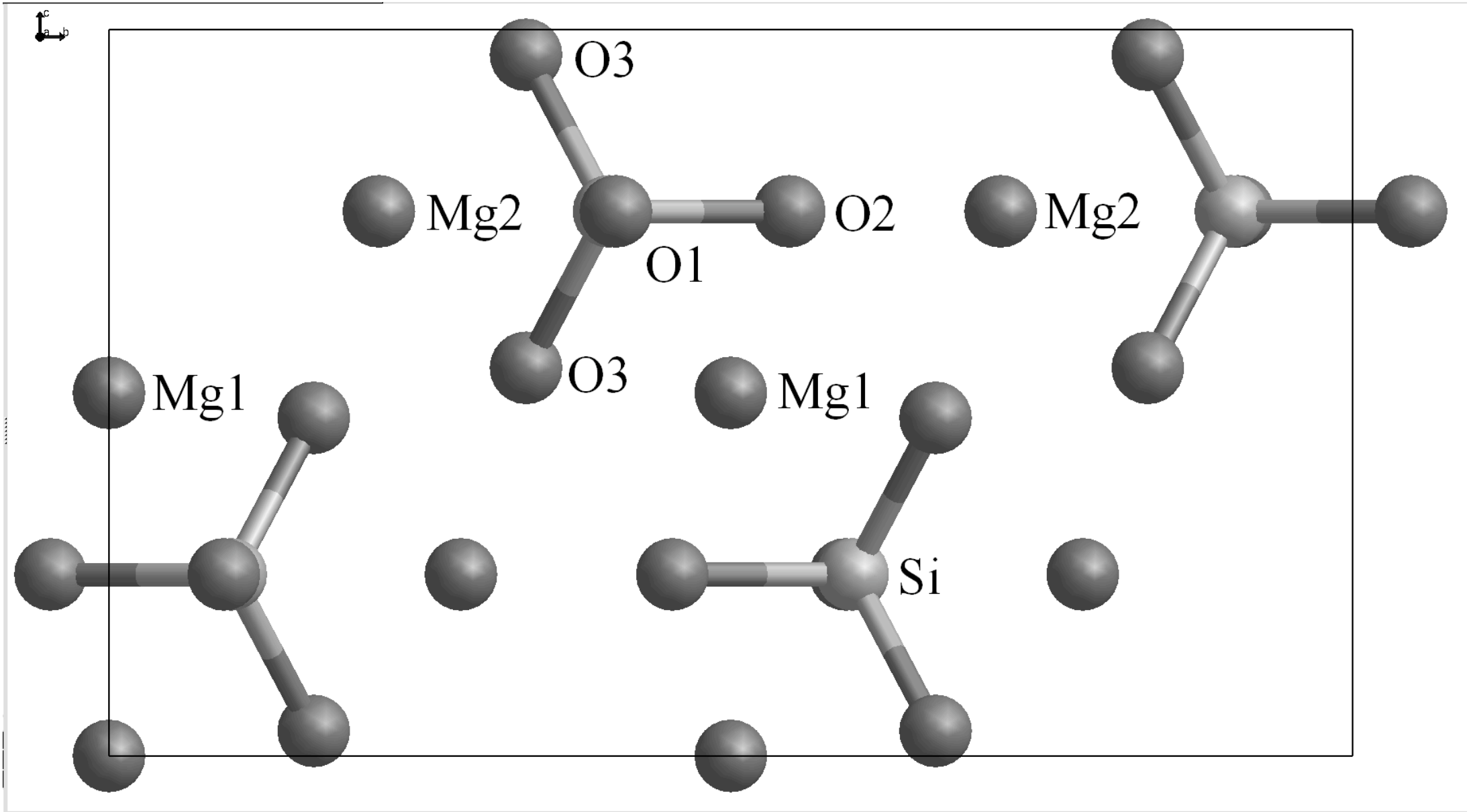
c
a
b
O3
Mg2
O2
O1
Mg2
O3
Mg1
Mg1
Si

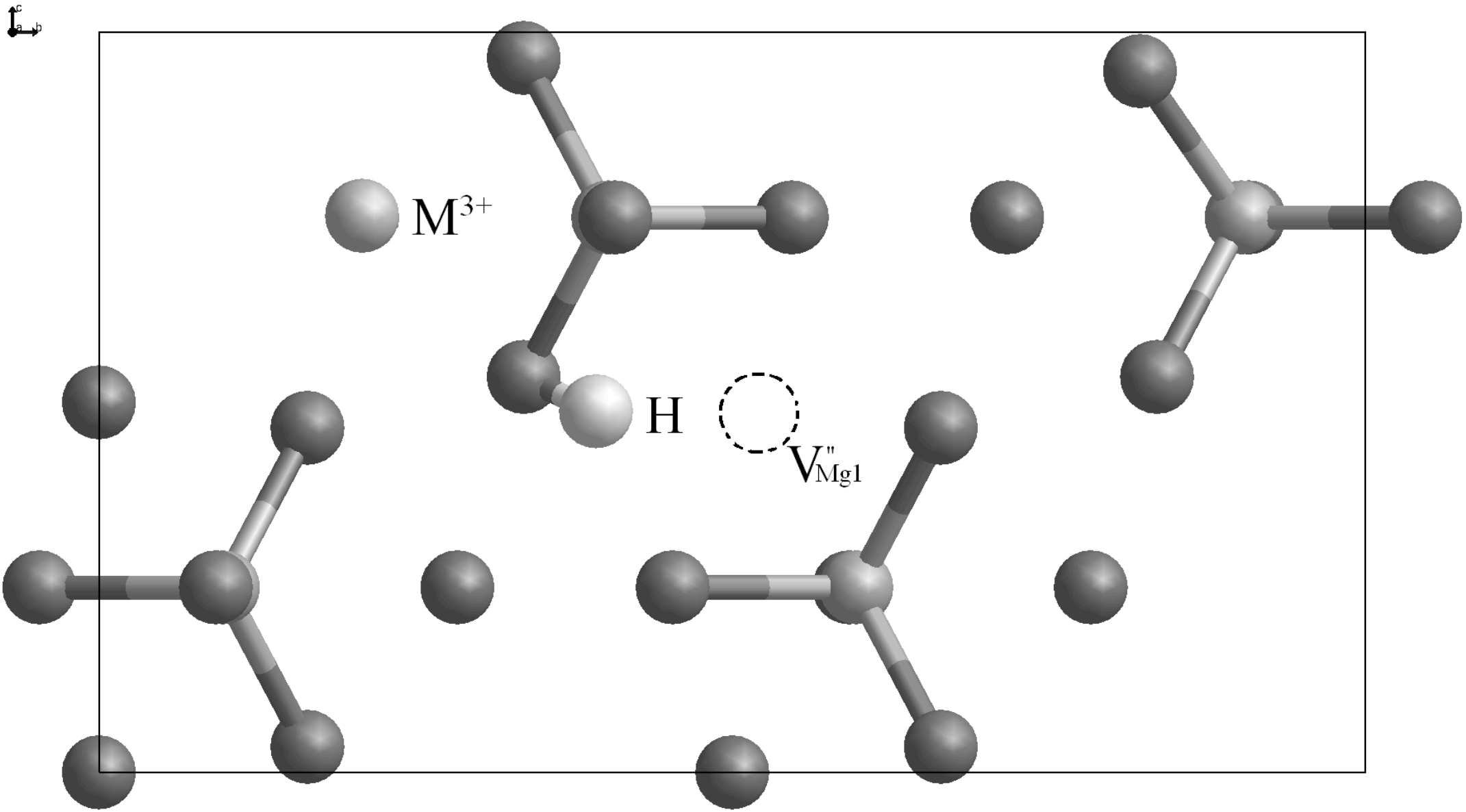
c
a
b
M^{3+}
H
V''_{Mg1}

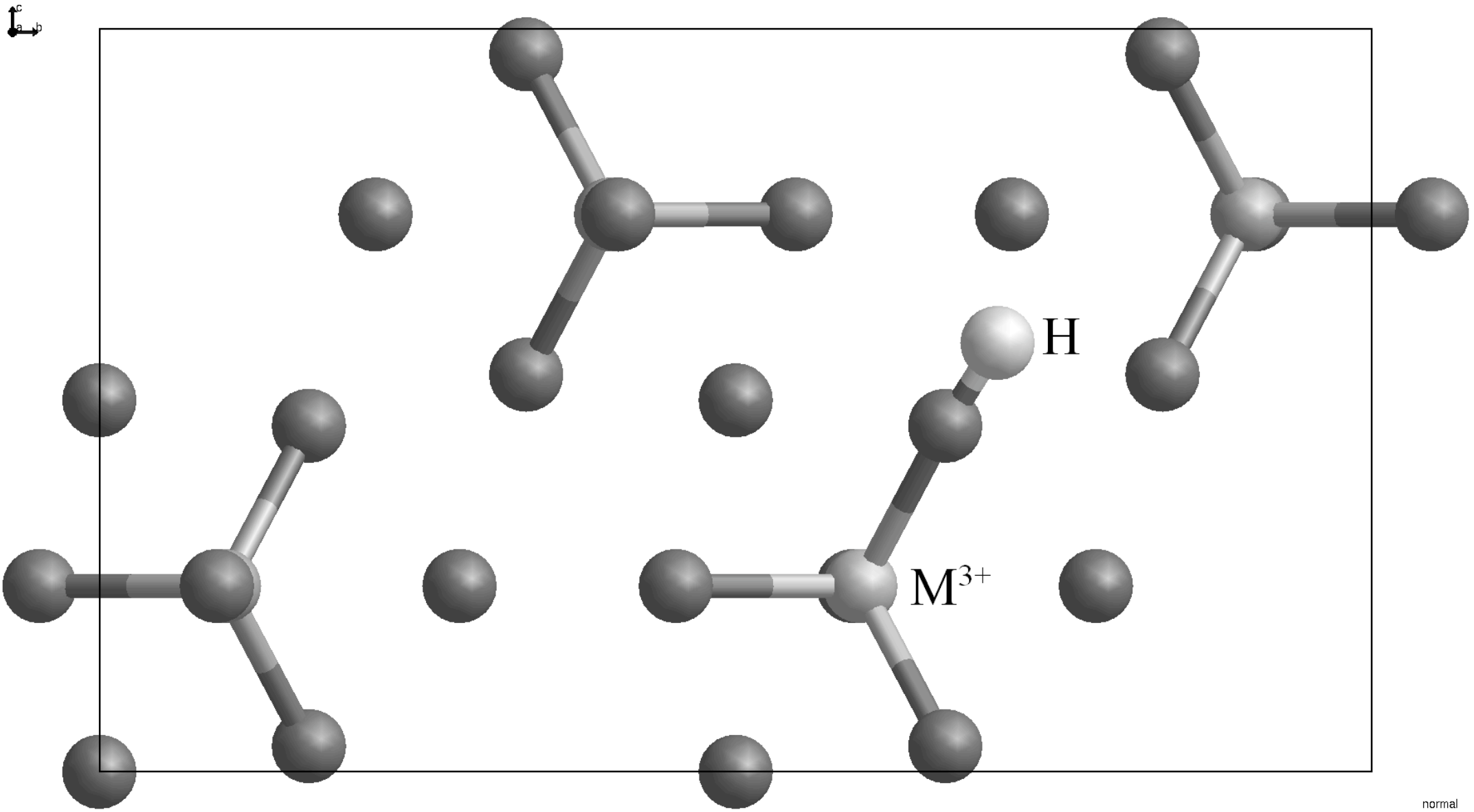
c
a
b
H
M3+
normal

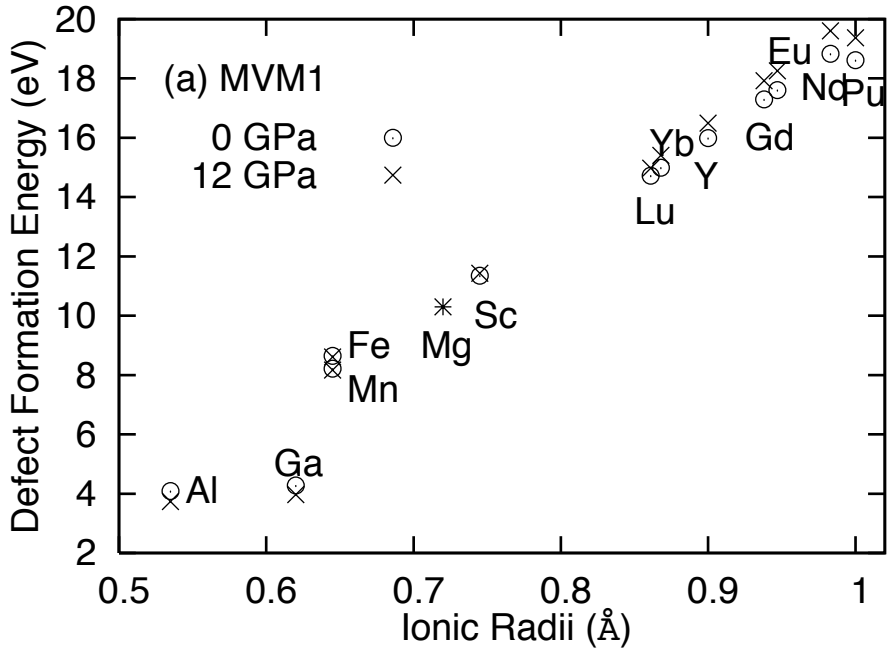
(a) MVM1
0 GPa
12 GPa
Defect Formation Energy (eV)
Ionic Radii (Å)
Al
Ga
Fe
Mn
Mg
Sc
Lu
Y
Yb
Gd
Eu
Nd
Pu

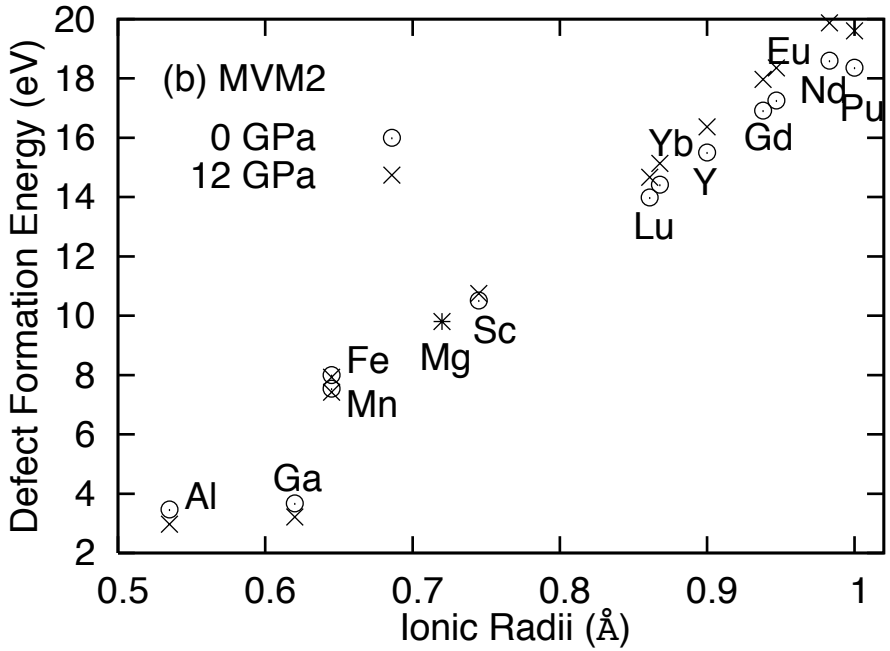
(b) MVM2
0 GPa
12 GPa
Defect Formation Energy (eV)
Ionic Radii (Å)
Al
Ga
Fe
Mn
Mg
Sc
Lu
Y
Yb
Gd
Eu
Nd
Pu

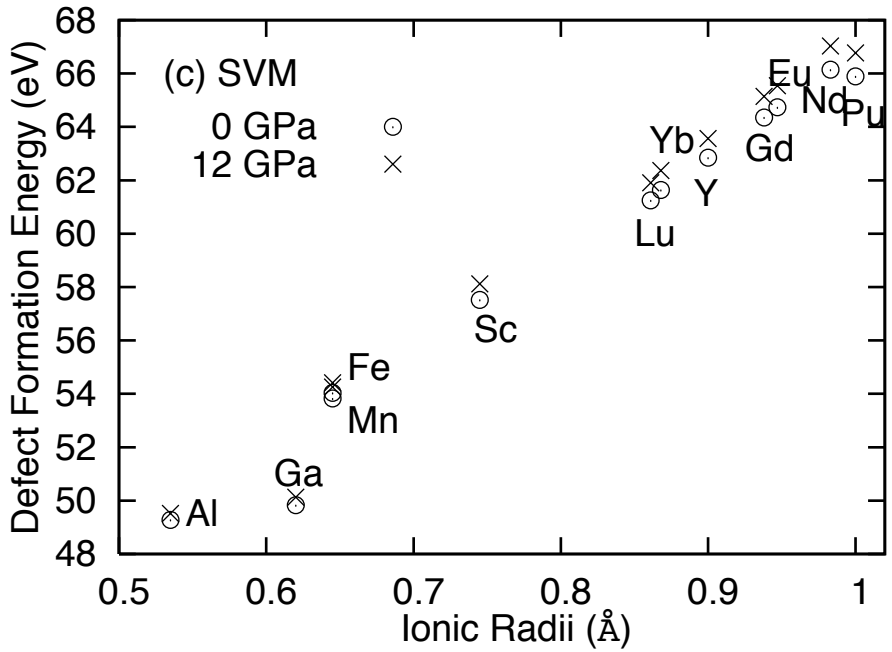
(c) SVM
0 GPa
12 GPa
Defect Formation Energy (eV)
Ionic Radii (Å)
Al
Ga
Fe
Mn
Sc
Lu
Y
Yb
Gd
Eu
Nd
Pu

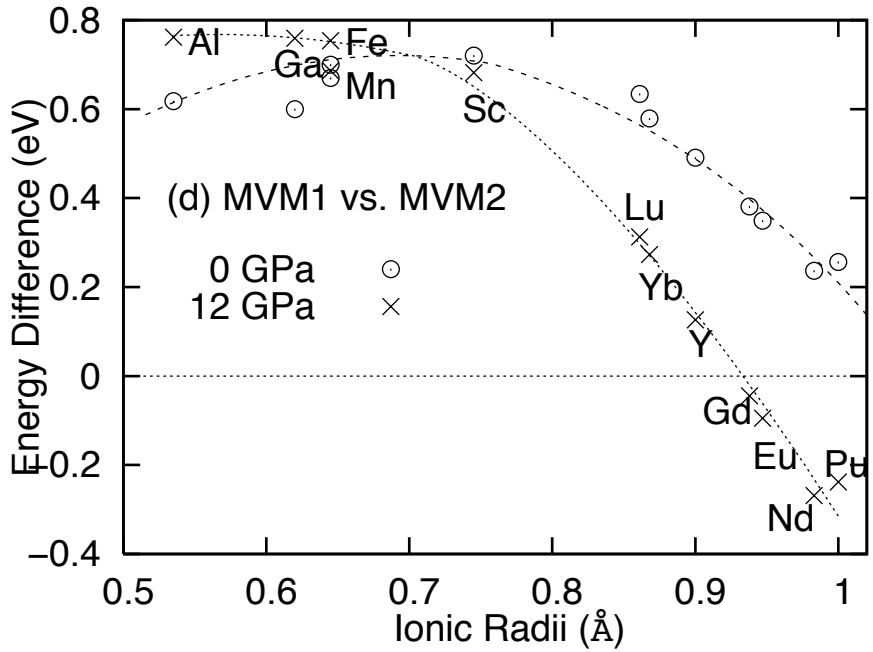
(d) MVM1 vs. MVM2
0 GPa
12 GPa
Energy Difference (eV)
Ionic Radii (Å)
Al
Ga
Fe
Mn
Sc
Lu
Yb
Y
Gd
Eu
Pu
Nd

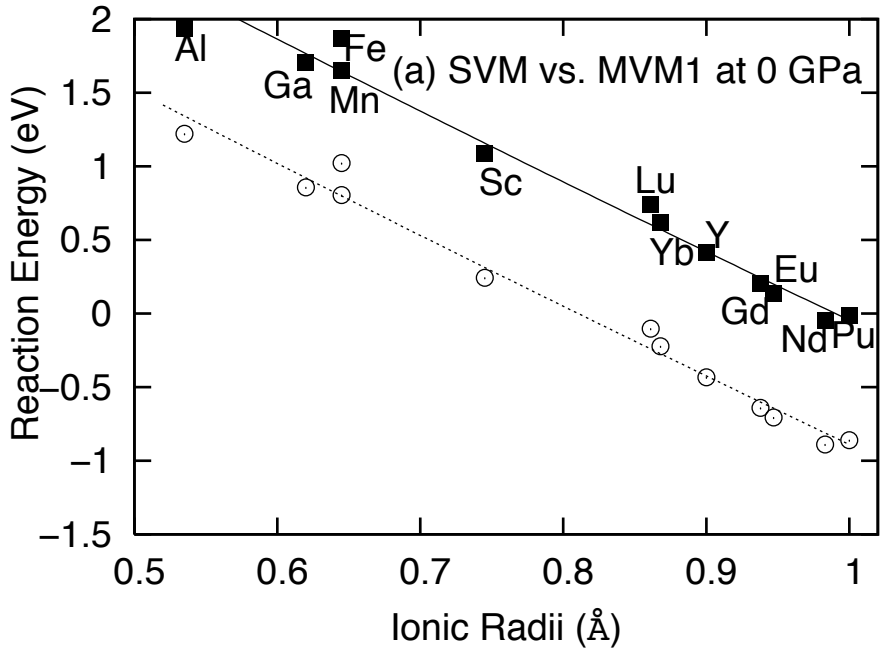
(a) SVM vs. MVM1 at 0 GPa
Reaction Energy (eV)
Ionic Radii (Å)
Al
Ga
Fe
Mn
Sc
Lu
Yb
Y
Eu
Gd
Nd
Pu

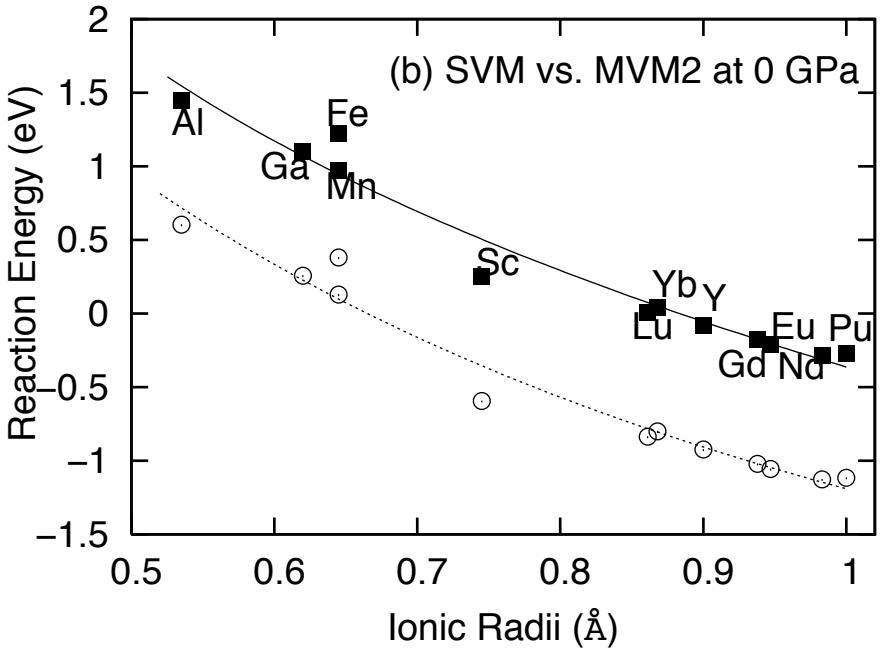
(b) SVM vs. MVM2 at 0 GPa
Reaction Energy (eV)
Ionic Radii (Å)
Al
Fe
Ga
Mn
Sc
Yb
Y
Lu
Eu
Pu
Gd
Nd

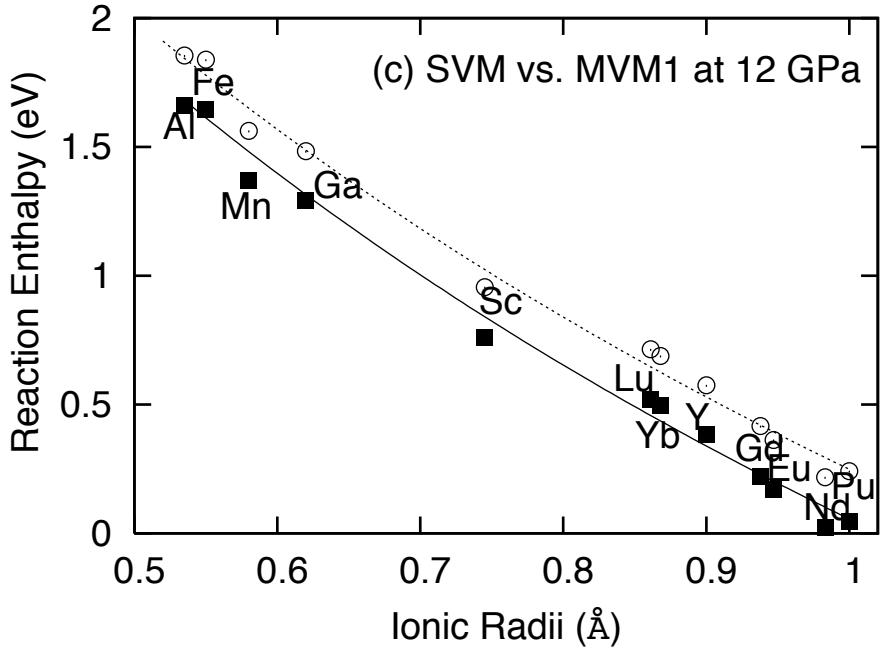
(c) SVM vs. MVM1 at 12 GPa
Reaction Enthalpy (eV)
Ionic Radii (Å)
Fe
Al
Mn
Ga
Sc
Lu
Y
Yb
Gd
Eu
Pu
Nd

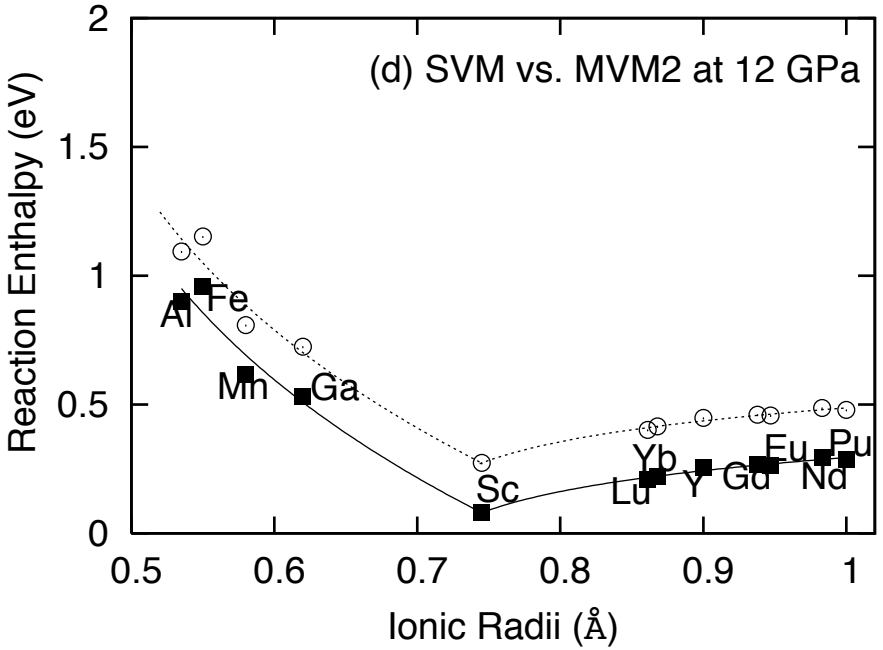
(d) SVM vs. MVM2 at 12 GPa
Reaction Enthalpy (eV)
Ionic Radii (Å)
Al
Fe
Mn
Ga
Sc
Yb
Lu
Y
Gd
Eu
Pu
Nd

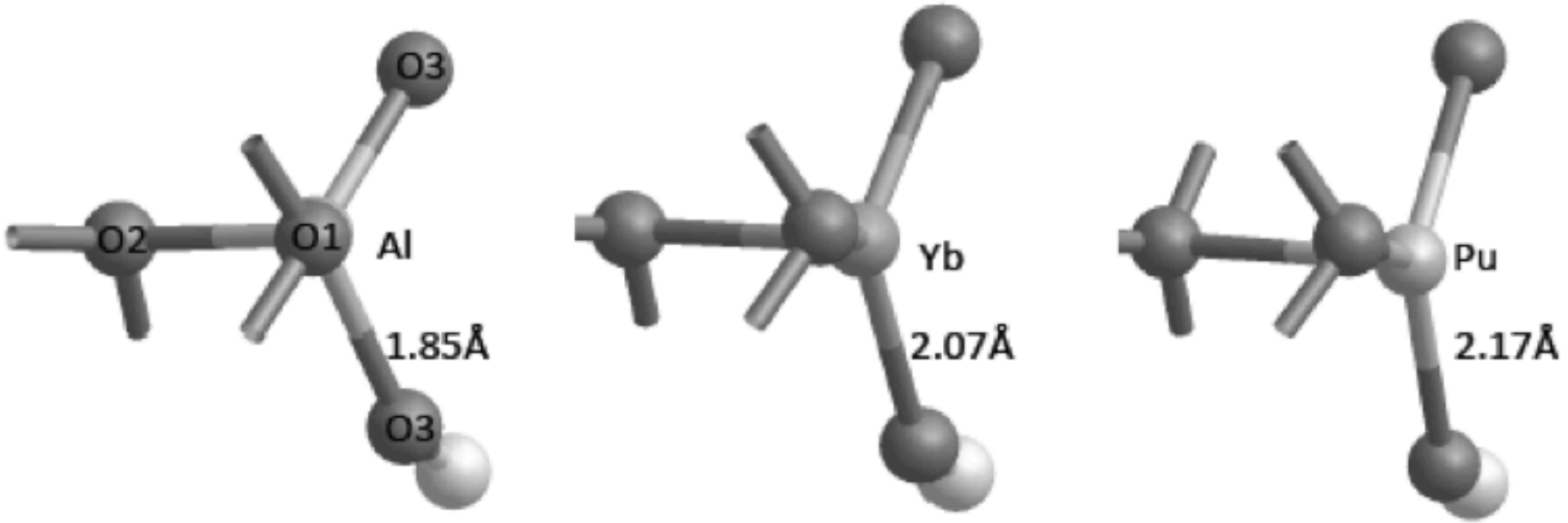
O3
O2
O1
Al
1.85Å
O3
Yb
2.07Å
Pu
2.17Å